Appl. Phys. A 77, 237–242 (2003)
DOI: 10.1007/s00339-003-2118-4

Applied Physics A
Materials Science & Processing

N. BÄRSCH✉
K. KÖRBER
A. OSTENDORF
K.H. TÖNSHOFF

Ablation and cutting of planar silicon devices using femtosecond laser pulses

Laser Zentrum Hannover e.V., Hollerithallee 8, 30419 Hannover, Germany

Received: 10 December 2002/Accepted: 20 January 2003
Published online: 28 May 2003 • **© Springer-Verlag 2003**

ABSTRACT Although lasers are generally able to machine silicon, the major material in many microsystems applications, doing so without influencing the physical properties of the bulk material remains an important challenge. Ultrafast lasers, in particular, with their potential to precisely ablate all kinds of solid materials, are able to perform such processes with high efficiency and accuracy. This article starts with an overview of the general interaction of ultrafast laser radiation with semiconductors, explaining the absorption processes and different fluence regimes for the ablation of silicon. Major parameter influences, especially for cutting processes in thin silicon, are described. By varying pulse energies, beam shaping methods, the beam polarization, and temperatures, the cutting quality and speed can be significantly influenced. One important quality aspect, besides kerf widths and surface roughness, is the amount of back-side chipping when cutting brittle materials. Achievements in speed enhancement using linear focus shapes are presented, with cutting speeds up to five times higher than by conventional spot-focusing. On the other hand, laser processes that cut with a spot focus offer the possibility of free-shape cutting, which is explained using the example of wafers carrying silicon chips with highly increased package densities.

PACS 52.38.Mf; 79.20.Ds; 81.05.Cy

1 Introduction

Microengineering processes play an essential role in daily life due to the continuous size reduction in many electronic devices. In many cases, common mechanical processes like sawing, drilling, or grinding have been adapted to micromechanical demands, but have come to their limits in the course of the progressing miniaturization. Specialized laser systems that are solely applicable to micro-material ablation offer alternative methods tailored to the processing of microelectronic and micromechanical components. For instance, when cutting thin wafers with mechanical blades, kerfs that are less than 10 μm wide cannot be realized with any state-of-the-art process due to the restrictions in the blade grain size and the mechanical forces involved. For the removal of only a few defined cubic micrometers of silicon from the surface of a delicate sensor, there is no mechanical process like milling available that might be able to handle materials with this precision.

Ultrashort pulsed lasers, due to their unique ability to precisely ablate materials, can process practically any solid substance with accuracies and resolutions that go down to the range of the laser wavelength or to the lattice dimensions. However, materials still behave differently from each other when ablated by femtosecond laser pulses. Silicon, as the most important material for the semiconductor industry, requires specific parameters to minimize cutting kerf widths, to reduce redeposition on the entrance surface, and to ensure a high kerf quality on all sides while retaining high processing speeds. This article explains the principle of material ablation with femtosecond lasers and describes beam parameters influencing the removal of material and the cutting process of silicon in particular.

2 Material ablation stimulated by fs laser pulses

2.1 *Beam–material interaction*

When ablating materials with lasers, the ablation rate is directly related to the absorption of light by the material. The absorption can be divided into interband and intraband processes. Interband absorption takes place when electrons are excited by photons with energies higher than the band gap energy E_g. The excitation can be done either by single-, two-, or multi-photon absorption. Since the Ti:sapphire laser wavelength of $\lambda = 780$ nm corresponds to a photon energy of $h\nu = 1.59$ eV, direct interband transitions, which, in the case of pure silicon, are possible for photon energies equal to or higher than 3.4 eV, require multiphoton absorption. On the other hand, the indirect band gap between two bands with different wave vectors amounts to $E_g = 1.12$ eV and can be overcome by a single photon, supported by phonons to change the wave vector. In any case, when electrons move from the valence to the conduction band due to any interband photon absorption, a hole and a free electron are generated. These both then participate in the ongoing process by intraband transitions, also described as free carrier absorption [1–3].

Since the interband transitions depend on the band gap, there is a major impact of the temperature and the doping level

✉ Fax: +49-511/2788-100, E-mail: nb@lzh.de

of silicon on the density of free carriers [1–6], as these parameters influence the band gap. Furthermore, the reflectivity of the material changes for intense laser pulses due to phase changes [1] and free carrier generation [2], thus again influencing the number of free carriers generated.

In addition to these primary processes between photons and electrons, excited electrons fall back from the conduction to the valence band in the course of secondary electron interactions, and give their energy to other electrons (Auger recombination). When focusing ultrashort laser pulses, the carrier density reaches values for which the energy absorbed by free carriers exceeds the energy absorbed by the lattice. Collisions between carriers begin to dominate collisions with the lattice and behave collectively as a plasma. The expression for the density of carrier pairs in (1) summarizes the energy transactions involved [1]:

$$N_{\mathrm{eh}}\frac{\partial}{\partial t}(E_{\mathrm{c}}) = I\left[\alpha_0\left(1-\frac{E_{\mathrm{g}}}{\hbar\omega}\right)+N_{\mathrm{eh}}\,\Sigma_{\mathrm{eh}}\right] + \frac{E_{\mathrm{g}}}{\tau_{\mathrm{R}}}\left[N_{\mathrm{eh}}-N_{\mathrm{eh}(T)}\right] + \nabla\left(E_{\mathrm{c}}D_{\mathrm{amb}}\nabla N_{\mathrm{eh}}\right)-\frac{N_{\mathrm{eh}}}{\tau_{\mathrm{e}}}\left(E_{\mathrm{c}}-\frac{3kT}{2}\right) \quad (1)$$

where N_{eh} is the density of carrier pairs, E_{c} is the energy of the carriers, α_0 is the absorption coefficient, Σ_{eh} is the absorption cross section of carrier pairs, E_{g} is the energy of the band gap, τ_{R} is the time for recombination, D_{amb} is the ambipolar diffusivity, τ_{e} is the time for carrier lattice relaxation, k is the Boltzmann constant, T is the substrate temperature, and the indices 'e' and 'h' correspond to 'electron' and 'hole', respectively.

The first term represents the energy gained from interband transitions and free carrier absorption. The second describes the energy liberated upon Auger recombination. The last two terms represent the energy loss by diffusing carriers and the energy transfer to the lattice, respectively.

For a description of absorption by intense laser pulses, the absorption coefficient α requires an extended examination. The most practicable extension considers the non-linear absorption [7]:

$$\alpha = \alpha_0 + \beta I \quad \text{with} \quad I = \frac{F}{\tau_{\mathrm{H}}} \quad (2)$$

where α_0 is the linear and βI the non-linear absorption, F is the fluence, and τ_{H} is the pulse duration. According to a measurement by Sokolowski-Tinten et al. for $\lambda = 625$ nm, the linear absorption of crystalline silicon is $\alpha_0 = 3.500\,\mathrm{cm}^{-1}$, and the two-photon absorption coefficient is $\beta = 55$ cm/GW in the case of 170 mJ/cm^2 [8]. There are also other descriptions for α in the literature, which are based either on the amount of free carriers [1] or on the temperature [3–5]. In any case, the absorption coefficient allows a first estimation of the optical penetration depth $\varrho = \alpha^{-1}$, which corresponds to the ablation depth when using the pulse energy at the ablation threshold. However, adequate values of the coefficients are not always available for the wavelength, the fluences, and the material under consideration, so experimental measurements of ablation rates are the most practical way for finding out real penetration depths.

2.2 *Ablation rates for silicon*

With regard to silicon, the ablation rates resulting from the specific beam–material interaction processes have been experimentally quantified both in low [7] and high [9] fluence regions. Figure 1 shows the measured ablation rate averages of 20 holes for each doping and pulse energy value, assuming that the focal plane always corresponds with the material surface [10]. The focal distance was 400 mm, using pulses of 150 fs at a wavelength of 780 nm.

For the regions of high fluence of up to several J/cm^2, which are reached when focusing pulses of several 100 µJ, the ablation depth per pulse has been quantified in relation to the pulse energy. The reasons for this are the surface roughness and the hole geometry, which keep changing the fluence during the multi-pulse ablation process. Single pulse ablation, on the other hand, does not cause significant material removal in relation to the error of known measurement methods.

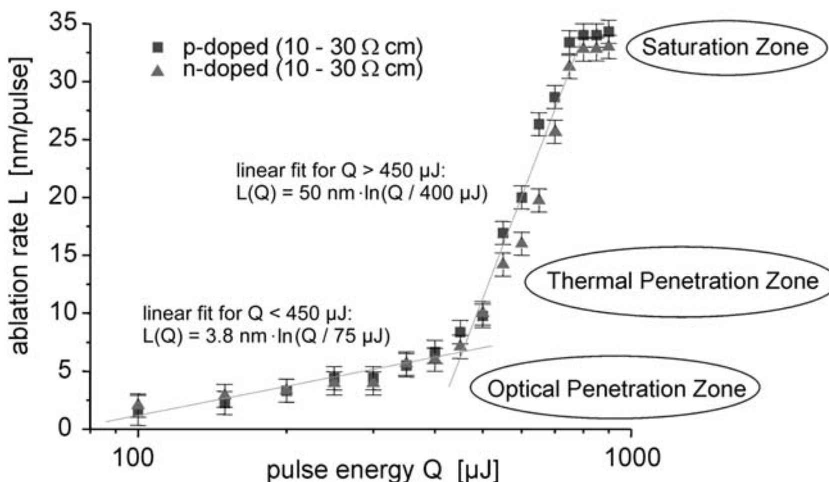

FIGURE 1 Ablation rate for Si (100) vs. pulse energy for a spot focal length of 400 mm [11]

The measurements verify the equation for the ablation rate L [7, 12]:

$$L = \varrho \ln \left(\frac{F}{F_{\text{th}}} \right), \tag{3}$$

where ϱ is the penetration depth, and the fluence F is defined as the quotient of the pulse energy Q and the illuminated area A, and F_{th} is the fluence at the ablation threshold. Three distinct areas in the diagram in Fig. 1 can be identified. At very high pulse energies (and fluences), a saturation effect can be observed, as L cannot be increased further. This is due to the short duration of the electron relaxation, which limits the area of energy transport processes by diffusion. In addition, the plasma from free electrons above the focus partially shields the material at higher fluences.

The two other areas represent the zones with optical and thermal penetration of the material as the respective major influences. An adjustment of (2) determines two different penetration depths given in Fig. 1 that are independent of the doping. The non-thermal ablation at fluences below $2.3\,\text{J/cm}^2$, corresponding to pulse energies of 450 μJ, results in an ablation rate of up to 5 nm per pulse. In the regime of thermal effects above $2.3\,\text{J/cm}^2$, the ablation rates then amount to 35 nm when using pulses with energies of almost 1 mJ. The reason for these two different ablation rate regimes can be found in the energy transport processes. When the density of free electrons, which increases at higher fluences, reaches a critical value of $10^{18}\,\text{cm}^{-3}$, collisions between the electrons begin to dominate other relaxation processes [1, 12]. This leads to slower energy transfer from the electrons to the lattice, enabling an energy transport to the bulk material by diffusion processes, in compliance with Sect. 2.1. When the evaporation temperature of 2628 K is exceeded, thermally induced ablation leads to increasing overall ablation rates, equivalent to a thermal penetration depth of 50 nm in the present case.

3 Cutting of thin silicon with fs laser pulses

3.1 *Experimental setup*

The femtosecond laser system used for the investigations emits ultrashort pulses at 780 nm with pulse durations of about 150 fs, pulse energies of up to 1 mJ, and a repetition rate of 1 kHz [13]. The beam quality is specified as $M^2 = 1.2$, the aperture being 6 mm. Focusing is done with various, usually achromatic lenses under incidence angles of 0° onto the sample surfaces, while the samples are moved with a 3-axes positioning system with accuracies below 1 μm.

3.2 *Major parameter influences*

Due to many additional influences, material ablation in processing applications is far more complex than single-pulse ablation. For example, drilling with femtosecond lasers by applying many pulses to the same spot involves reflection effects at the borders of partially drilled holes [14]. Furthermore, ablation rates change as the material surface changes its topography and physical properties once the drilling process has started. With regard to cutting processes, there are even more relevant influences. Moving a sample under static laser pulses at 1 kHz, focused to a diameter of about 50 μm, results in a pulse overlap at feed rates of up to about 50 mm/s. Common processing speeds for micromechanical applications in the range of 1 mm/s therefore lead to large pulse overlaps with a strong influence on the ablation process for each pulse, as asymmetrical reflections occur at the borders of a partially cut kerf.

Within the few last years, the processing of various solid materials with femtosecond lasers has been studied, of which silicon is one with an especially large range of applications, due to its importance both for microelectronic and micromachining applications. The cutting of ultrathin silicon is an especially important field in which femtosecond lasers have the potential to become a competitive tool. Therefore, investigations of the cutting of thin silicon must also focus on cutting with high pulse energies of up to 1 mJ, although the best cutting qualities are achieved using low pulse energies in the regime of mere non-thermal ablation (Fig. 1).

As parameters of major influence on the processing of thin silicon, the material thickness, the pulse energy, and the beam shape have been identified. The substrate temperature is also relevant, as cutting speeds have been shown to increase by up to 50% compared to room temperature when cutting silicon at temperatures of 300 to 400 °C [10]. However, the processing of thin wafers at temperatures higher than 100 °C is usually impossible due to preconditions in connection with wafer handling.

Further parameters that are especially important when considering linear cutting are the polarization of the laser beam and the crystal orientation of the material, but these both have been shown not to influence the cutting speed. While there is almost no influence at all from the crystal orientation, the beam polarization does have a major influence on the exit surface quality of the cuts. Figure 2 demonstrates this depen-

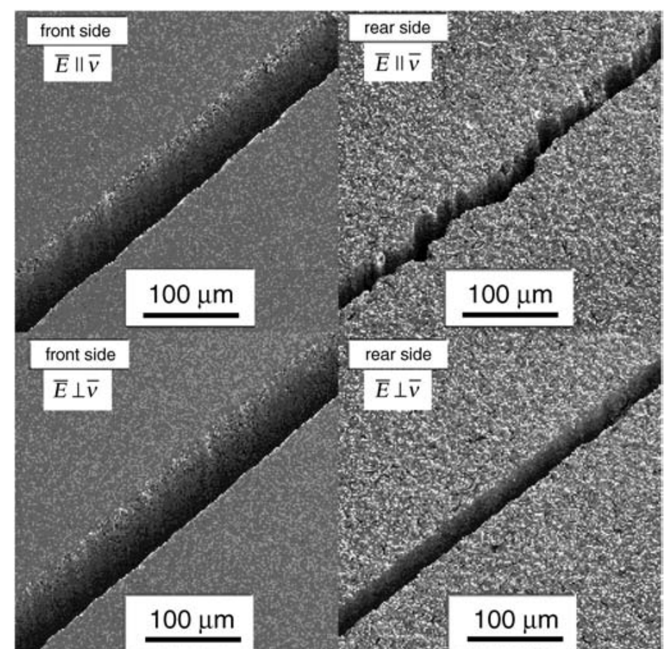

FIGURE 2 Laser entrance and exit surfaces of 100 μm thick silicon at different polarizations [15]

dence of the kerf quality on the polarization of the laser beam when cutting with standard focusing optics for the example of 380 μm thick silicon, cut with pulse energies of 400 μJ at an effective cutting speed of 0.5 mm/min [15]. The results show the best quality when cutting vertically to the polarization direction. This is due to the dependence of the reflectivity on the angle of incidence according to Fresnel. Especially in the range of 60° to 90°, the reflectivity is different for vertical (index 'v') and parallel (index 'p') polarizations, as shown in Fig. 3, based on the equations for the reflection q_r [10, 16]:

$$q_{r,v} = \frac{E_{r,v}}{E_{0,v}} = \frac{\left(\sqrt{n_0^2 - \sin^2\alpha_1 - \cos\alpha_1} - \cos\alpha_1\right)^2}{n_0^2 - 1}, \qquad (4)$$

$$q_{r,p} = \frac{E_{r,p}}{E_{0,p}} = \frac{n_0^2\cos\alpha_1 - \sqrt{n_0^2 - \sin^2\alpha_1}}{n_0^2\cos\alpha_1 + \sqrt{n_0^2 - \sin^2\alpha_1}}, \qquad (5)$$

with q_r being the reflection coefficient and E_r the reflected part of the energy E_0, each given for polarizations vertical and parallel to the material surface. α_1 is the incidence angle and n_0 the linear refraction index. In both cases, the polarization is vertical to the spreading direction of the laser beam, as shown in Fig. 3.

Due to the higher intensity in the center of the beam, the formation of kerfs with side angles below 90° is normal for material ablation with a Gaussian beam shape. The polarization dependence of the reflection especially for angles around 70° to 80° leads to inhomogeneous kerf development for polarizations parallel to the cutting direction [10]. In practice, a continuous rotation of the polarization using a rotating half-wave plate in the beam path has been shown to be an effective measure for reducing such irregularities.

A second effect with a major impact on the cut exit surface, besides the polarization effect discussed above, is the so-called chipping effect, which can be observed strongly in the cut shown in Fig. 4. The cut was machined with a pulse energy of 400 μJ in a 50 μm thin wafer using a feed rate of 70 mm/min. When the material has not yet been completely cut through by the laser pulses, the remaining layer is burst away by the influence of the plasma, especially when working in a normal atmosphere. This effect can be suppressed to a great extent by adapting common process parameters like pulse energy, feed rate, number of repetitions, and the position of the focal plane. Especially when cutting a silicon wafer in one step with low feed rates, there is a distinct transition with regard to chipping between feed rates that suffice for a complete cut through the wafer, and feed rates that leave

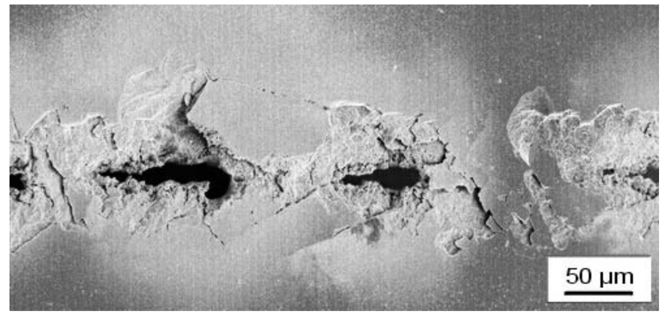

FIGURE 4 Chipping effect when cutting thin silicon incompletely with high feed rates

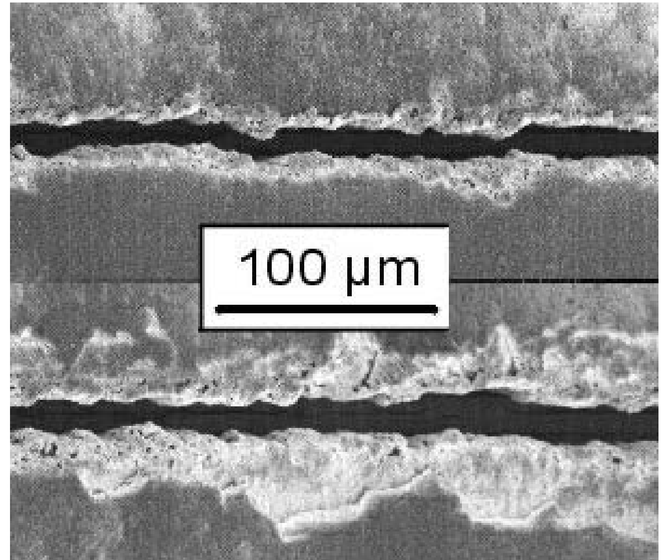

FIGURE 5 Chipping effect when cutting 50 μm thin silicon with a spot focus using lower feed rates (little chipping) and higher feed rates (strong chipping)

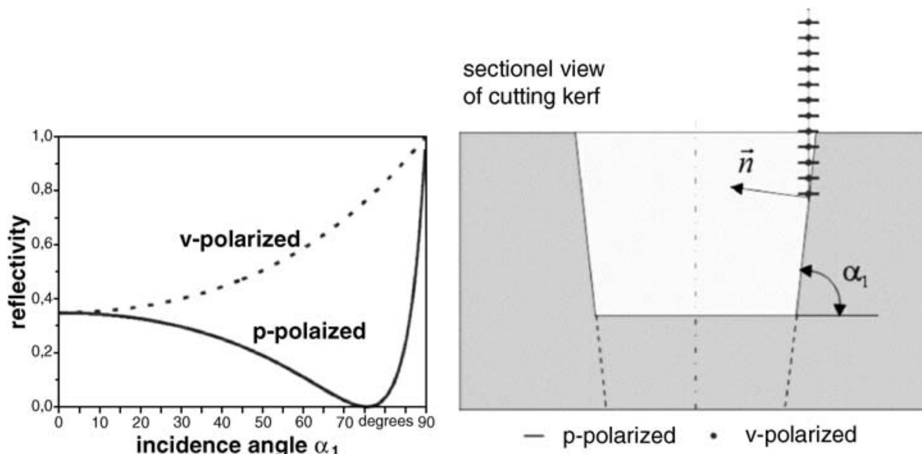

FIGURE 3 Reflection for crystalline silicon and linear polarization of laser pulses at $\lambda = 780$ nm [11]

a remaining layer of material that is burst away by the plasma pressure and oscillation effects. Figure 5 shows the difference for the example of a 50 μm thin wafer cut with fs laser pulses with energies of 400 μJ: the upper cut (little chipping) was done at a feed rate of 40 mm/min, the lower cut (strong chipping) at 50 mm/min.

This suppression of chipping effects always goes along with a minor speed decrease compared to the maximum speed enabling the separation of a wafer, which also contributes to the necessity for finding ways to speed the cutting process up. Investigations have shown that beam shaping has the greatest potential for further improvements of the cutting process in many respects and particularly with regard to speed enhancements. The following section describes the latest investigations.

3.3 *Cutting with alternative focusing shapes*

The conventional spot focus produced by achromatic lenses enables femtosecond lasers to do precise cuts of any shape, as demonstrated by the trepanned structures of a hole and a micro-gearwheel in silicon shown in Fig. 6. These structures were cut with pulse energies of 200 μJ at effective cutting speeds of 0.6 mm/min.

Linear cuts, on the other hand, can also be realized with different focusing strategies. The latest investigations have shown that when cutting with line foci instead of spot foci using a system of cylinder lenses for the beam shaping, cutting speeds can be multiplied by factors of five for linear cuts, and kerf widths can be significantly reduced at the same time. An assembly like that shown in Fig. 7 allows a flexible focus shape adjustment by an easy lens distance variation: a larger distance between the focal planes leads to an increase of the focus line length.

When laser pulses are focused to certain lines with lengths of up to several millimeters and widths of only a few micometers, the energy input into the material is improved due to a larger pulse overlap and a better fluence distribution – provided that the alignment of the focal line and the cutting direction of the stages correspond exactly, and that the ablation threshold of the material is still overcome by the fluence within the major area of the line focus.

The high quality that can be achieved by static line focusing without movement of the workpiece is demonstrated by Fig. 8, which shows a kerf that was cut through the whole of a piece of 50 μm thin silicon by exposing it to a line focus with a length of 2 mm, using femtosecond laser pulses as specified in Sect. 3.1. However, a vast improvement of the cutting speeds compared with conventional spot focusing with achromatic lenses is only achieved with line foci whose fluence distribution is optimized with regard to the ablation threshold and the given pulse overlap. This optimization is influenced by various parameters. Experimental results show that for a cylindrical focal length of about 70 mm, a focal line with a length around 500 μm produces kerf widths of 10 to 15 μm

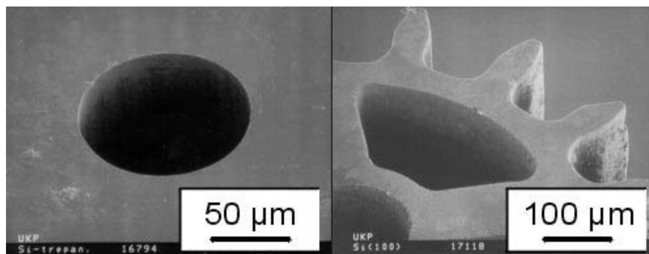

FIGURE 6 Examples of silicon structuring with fs laser pulses by trepanning with a spot focus

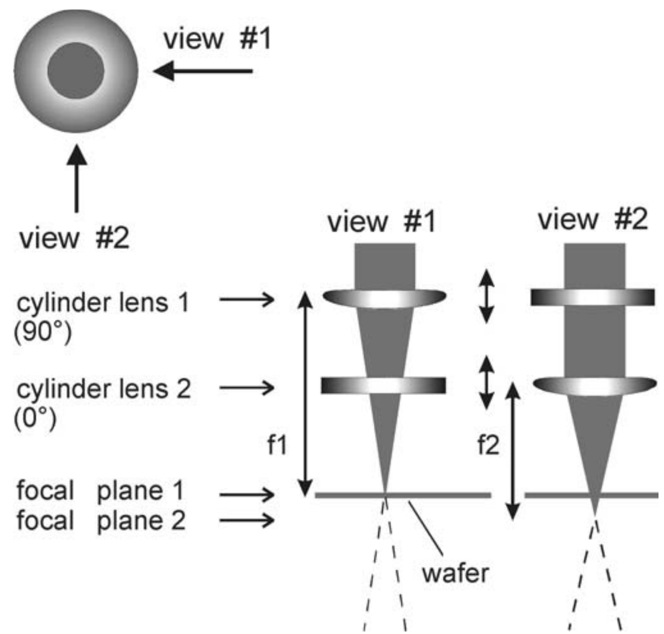

FIGURE 7 Principle of line focus generation to enhance linear cutting speeds

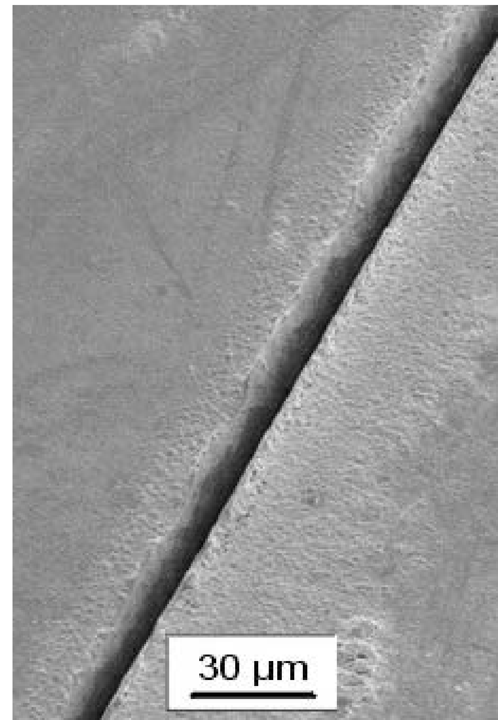

FIGURE 8 Kerf in thin silicon, cut by static exposure to fs laser pulses shaped to a line focus

and leads to the highest cutting speeds when moving the silicon workpiece in the direction of the kerf. The maximum cutting speed that could be achieved was 550 mm/min, whereas achromatic spot foci with focal lengths of 50 to 80 mm result in cutting speeds of up to about 100 to 150 mm/min using the same material and laser source.

On the other hand, for those applications in which the cutting speed plays a minor role, femtosecond lasers not only provide the highest accuracies, the lowest achievable structure sizes, and the best surface qualities, but also enable any random, non-linear shape to be cut using common spot focusing optics. On the other hand, conventional abrasive cutting methods with diamond blades, as well as laser cutting methods with linear foci, are restricted to straight linear cuts. When cutting through thin silicon with femtosecond pulses focused to a spot in the range of 10 to 50 μm, elements with a large range of shapes can be cut out, either adapted to a special function or to minimize the component size and to increase the packing density. For instance, when cutting out hexagonal shapes with the same diameter as rectangular dice, their packing density on a wafer can be increased by 43% (Fig. 9) [9, 10]. In this field, femtosecond lasers offer new opportunities for the design of silicon wafers that have so far been limited by conventional linear cutting methods.

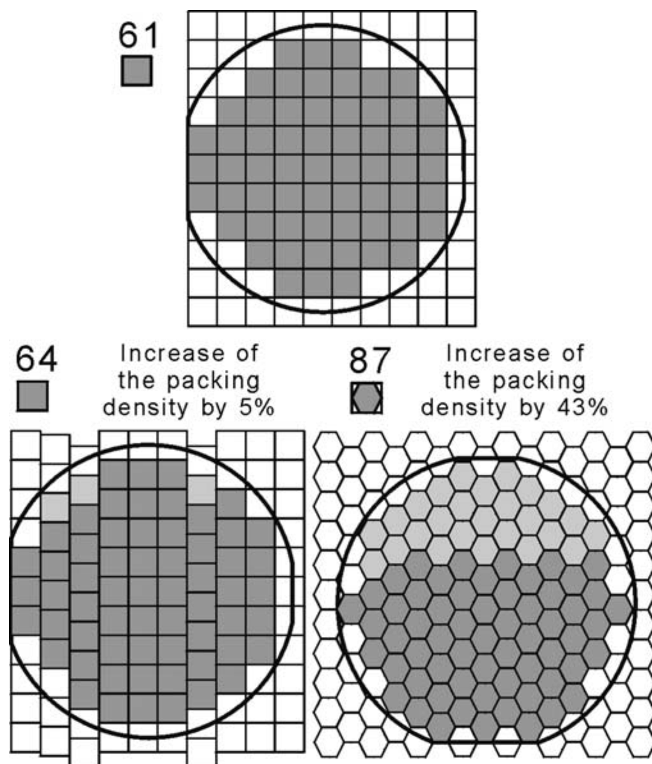

FIGURE 9 Examples of increasing the lateral density of elements using non-rectangular geometries when cutting with a spot focus [15]

4 Conclusion/outlook

It has been shown that for the processing of crystalline silicon, ultrashort-pulsed lasers are a tool with a promising future, particularly in the field of small lot sizes and highly complex geometries. The cutting of thin silicon can be performed with higher accuracy and smaller cutting kerfs than by any conventional cutting method, and due to the ability to cut free shapes, it offers new ways to design electronic components. When higher cutting speeds become necessary, the use of line foci created by systems of cylinder lenses leads to considerable speed enhancements for linear cuts and has the potential for further cutting speed increases. An example of a precise line focus cut has been presented and possibilities for wafer dicing using such focusing strategies have been illustrated.

Since new femtosecond laser systems with higher average powers, even at lower pulse energies, are being developed, cutting thin silicon is expected to become even faster and more precise in the near future, as higher average powers lead to cutting speed increases and lower pulse energies to more accurate cuts. With a basic knowledge of the ablation process and its important parameters and enhancement options, as presented in this paper, the cutting of silicon – as well as other applications in the field of semiconductor processing – can be continuously improved. Further progress can be expected with the next generations of femtosecond laser systems on the market.

ACKNOWLEDGEMENTS This work was financed by the European Community in the Growth programme (GRD1-2000-25380).

REFERENCES

1 M. von Allmen, A. Blatter: *Laser-Beam Interactions with Materials*, 2nd edn. (Springer, Heidelberg 1998)
2 D. von der Linde, K. Sokolowski-Tinten, J. Bialkowski: Appl. Surf. Sci. **109/110**, 1 (1997)
3 H.-J. Bargel, P. Cardinal, H. Hilbrans, K.-H. Hübner, G. Schulze, G. Wurzel: *Werkstoffkunde*, 7th edn. (Springer, Heidelberg 2000)
4 J. Weber: *Properties of Crystalline Silicon* (INSPEC, London 1999)
5 B.K. Sun, X. Zhang, C.P. Grigoropoulos: Int. J. Heat Mass Transfer **40**, 7 (1996)
6 S.M. Sze: *Physics of Semiconductor Devices* (John Wiley, Singapore 1981)
7 W. Kautek, J. Krüger: Proc. SPIE **2207**, 600 (1994)
8 K. Sokolowski-Tinten, J. Bialkowski, D. von der Linde: Phys. Rev. B **51**, 14 186 (1995)
9 H.K. Tönshoff, A. Ostendorf, K. Körber, T. Wagner: Proc. ICALEO 2000 in Dearborn, USA, 2000
10 T. Wagner: *Abtragen von kristallinem Silizium mit ultrakurzen Laserpulsen* (Thesis, Hannover 2002)
11 C. Momma, S. Nolte: Appl. Surf. Sci. **109/110**, 15 (1997)
12 J. Bialkowski: *Femtosekundenlaser-induzierter Materialabtrag* (Thesis, Essen 2000)
13 Clark-MXR, Inc.: CPA-2001 amplified kHz Ti:Sapphire Laser System; http://64.227.154.50/Scientific/CPA2001.htm (Dexter, 2001)
14 S. Nolte, C. Momma, G. Kamlage, A. Ostendorf, C. Fallnich, F. von Alvensleben, H. Welling: Appl. Phys. A **68**, 563 (1999)
15 H.K. Tönshoff, A. Ostendorf, T. Wagner: Proc. SPIE **4274**, 88 (2001)
16 L. Bergmann, C. Schaefer: *Optik*, 9th edn. (Gruyter, Berlin 1993)